Quantifying uncertainties due to irreducible three-body forces in deuteron-nucleus reactions

L. Hlophe ⬤,[*] K. Kravvaris, and S. Quaglioni

Lawrence Livermore National Laboratory, P.O. Box 808, L-414, Livermore, California 94551, USA

Background: Deuteron-induced nuclear reactions are an essential tool for probing the structure of nuclei as well as astrophysical information such as (n, γ) cross sections. The deuteron-nucleus system is typically described within a Faddeev three-body model consisting of a neutron (n), a proton (p), and the target nucleus (A) interacting through pairwise phenomenological potentials. While Faddeev techniques enable the exact description of the three-body dynamics, their predictive power is limited in part by the omission of irreducible neutron-proton-nucleus three-body force (n-p-A 3BF).

Purpose: Our goal is to quantify systematic uncertainties stemming from the reduction of deuteron-nucleus ($d + A$) dynamics to a picture of three pointlike nuclear clusters interacting via pairwise nucleon-nucleus forces, using as testing grounds $d + \alpha$ scattering and the ^{6}Li ground state. We particularly focus on quantifying uncertainties arising from the full antisymmetrization of the $(A + 2)$-body system with the target nucleus fixed in its ground state.

Methods: We adopt the *ab initio* no-core shell model coupled with the resonating group method (NCSM/RGM) to compute microscopic n-α and p-α interactions, and use them in a three-body description of the $d + \alpha$ system by means of momentum-space Faddeev-type equations. Simultaneously, we also carry out *ab initio* calculations of $d + \alpha$ scattering and ^{6}Li ground state by means of six-body NCSM/RGM calculations to serve as a benchmark for the three-body model predictions given by the Faddeev calculations.

Results: By comparing the Faddeev and NCSM/RGM results, we show that the irreducible n-p-α 3BF has a non-negligible effect on bound state and scattering observables alike. Specifically, the Faddeev approach yields a ^{6}Li ground state that is approximately 600 keV shallower than the one obtained with the NCSM/RGM. Additionally, the Faddeev calculations for $d + \alpha$ scattering yield a 3^+ resonance that is located approximately 400 keV higher in energy compared to the NCSM/RGM result. The shape of the $d + \alpha$ angular distributions computed using the two approaches also differ, owing to the discrepancy in the predictions of the 3^+ resonance energy.

Conclusions: The Faddeev three-body model predictions for $d + \alpha$ scattering and ^{6}Li using microscopic n-α and p-α potentials differ from those computed microscopically with the NCSM/RGM. These discrepancies are due to the n-p-α 3BF, which arises from two-nucleon exchange terms in the microscopic d-α interaction and are not accounted for in the three-body model Faddeev calculations. This study lays the foundation for future parametrizations of the 3BF due to Pauli exclusion principle effects in improved three-body calculations of deuteron-induced reactions.

I. INTRODUCTION

Deuteron-induced nuclear reactions are powerful tools for probing the properties of nuclei, especially for short-lived exotic isotopes for which direct measurements are unfeasible. Additionally, combining experimental measurements with an accurate reaction theory provides means for determining nuclear structure information as well as capture rates that are needed for astrophysical nucleosynthesis modeling. An *ab initio* description of such deuteron-induced reactions requires the solution of the many-body scattering problem, which at this time is only feasible for light systems with up to nine nucleons [1,2]. To overcome this limitation, deuteron-induced scattering and reactions on a target nucleus (A) are typically treated

within a three-body model consisting of a dynamically inert core, a proton (p), and a neutron (n) interacting through an effective three-body Hamiltonian, such that an exact solution can be obtained through the Faddeev formalism [3]. While simplified numerical approaches have been applied with varying degrees of success [4–6], the use of the Faddeev formalism eliminates additional errors due to approximate treatment of three-body dynamics.

Typically, the effective three-body Hamiltonian is approximated as a direct sum of the pairwise interactions of the subsystems, namely, the n-p, n-A, and p-A potentials. The n-p potential is usually constrained by high-precision fits to nucleon-nucleon (NN) elastic scattering data. Commonly adopted models are, for example, the Bonn [7,8] or chiral effective theory [9–11] (χEFT) potentials. Local phenomenological nucleon-nucleus ($\mathcal{W}_{NA}$) potentials constrained using elastic scattering data have been successfully applied to describe

_____

*hlophe1@llnl.gov

deuteron-induced reactions on targets ranging from the lightest nuclei, e.g., the deuteron [12] to much heavier nuclei such as nickel [13]. However, such nucleon-nucleus (N-A) potentials are not uniquely defined and, as a result, different functional forms provide accurate fits to $N + A$ scattering data but yield different predictions for the deuteron-nucleus ($d + A$) systems [14–16]. Further, insights from microscopic reaction theory revealed that the nucleon-nucleus potentials are generally nonlocal and dispersive [17]. The works of Ref. [15,18] demonstrated that nonlocality significantly impacts predictions for $d + A$ reaction observables. Moreover, it was shown in Ref. [19] that imposing dispersivity leads to improved nucleon-nucleus potentials that consistently describe both the bound and scattering states for the $N + A$ system. Finally, the formal projection of the $(A + 2)$-body problem onto the three-particle space produces not only pairwise potentials but also an irreducible effective three-body force (3BF). To improve the predictive power of the three-body model it is thus necessary to investigate the origin of this 3BF and assess its impact on properties of the $d + A$ system. Past attempts to quantify the effects of the 3BF on deuteron-induced reaction observables based on simplified nuclear structure and reaction models [20–23] have been made. More recent investigations along these lines have been carried out in Ref. [24], where the 3BF emerges from interactions between the neutron and proton via excitation of the target A. In Ref. [25] several bound systems (^{6}He $= \alpha + n + n$, ^{9}Be $= \alpha + \alpha + n$, ^{12}C $= \alpha + \alpha + \alpha$) were studied using the no-core shell model coupled with the resonating group method (NCSM/RGM) starting from phenomenological nucleon-nucleon (NN) forces, where the α particle was fixed in its ground state so that only antisymmetrization contributions to the 3BF were captured. The results of the three-body model were found to consistently lead to smaller binding energies when compared to the fully microscopic calculations.

In the present work we investigate the irreducible 3BF in a light nuclear system and quantify its effects on both bound-state and scattering observables using as a test case the $d + \alpha$ system. Our objective is to isolate contributions to the 3BF arising from the Pauli exclusion principle, disentangling them from other mechanisms such as target excitation and three-nucleon (3N) forces. Starting from a five-nucleon Hamiltonian based on the χEFT NN interaction of Ref. [9,10] softened with a similarity renormalization group (SRG) transformation [26] (in two-body space), momentum-space nonlocal microscopic n-α ($\mathcal{W}_{n\alpha}$) and p-α ($\mathcal{W}_{p\alpha}$) potentials are computed working within the framework of the NCSM/RGM [27,28]. For the purpose of the present study, we restrict the four nucleons within the α particle to the ground state. These nonlocal, momentum-space $\mathcal{W}_{N\alpha}$ potentials are then used together with the SRG-evolved χEFT n-p interaction within the Faddeev formalism to make predictions for the $d + \alpha$ system. To overcome the limitations of the screening and renormalization approach introduced in Ref. [29], which is valid only in regions where the effects of the $p + A$ Coulomb potential are relatively weak (i.e., at high energies or in light nuclei) [30], here we utilize a new capability [31] based on the Alt-Grassberger-Sandhas (AGS)

[32] formulation of the Faddeev equations in a basis of $p + A$ Coulomb scattering wave functions [33]. Simultaneously, we also apply the (six-body) NCSM/RGM approach to directly compute $d + \alpha$ bound and scattering observables starting from the same χEFT NN interaction. By comparing the Faddeev and NCM/RGM results, we show that the irreducible 3BF owing to microscopic antisymmetrization effects has a small but significant impact on the ^{6}Li bound state and $d + \alpha$ scattering, accounting for 600 keV of the binding energy and shifting the 3^+ resonance by $\approx$400 keV lower in energy.

This paper is organized as follows. In Sec. II A we present a brief summary of the Faddeev-AGS equations in the Coulomb basis. An overview of the momentum space NCSM/RGM needed to evaluate the effective N-A potentials is provided in Sec. II B and a detailed discussion with explicit expressions for the potentials is given in Appendix. In Sec. III, we discuss our results for $d + \alpha$ scattering and ^{6}Li bound-state calculations, and assess the effect of the irreducible three-body force by comparing results obtained within the Faddeev-AGS approach with those computed directly with the NCSM/RGM. The conclusion and outlook are given in Sec. IV.

II. FORMALISM

A. Faddeev formalism with exact treatment of the average Coulomb potential

The scattering of a deuteron from a target nucleus A leading to all possible three-body rearrangement processes (see Fig. 1) can be consistently described using the Faddeev formalism. It is convenient to assign numerical labels $\{1, 2, 3\}$ to the particles $\{A, p, n\}$, respectively, and to define corresponding arrangement channels $i = 1, 2, 3$ consisting of a spectator particle i and the remaining particle pair interacting through their respective pairwise potential $\mathcal{W}_i$. For example, arrangement channel 1 contains an interacting $n + p$ pair with a spectator A, where $\mathcal{W}_1 \equiv V^{np}$. Similarly, $\mathcal{W}_2 \equiv \mathcal{W}^{nA}$, and $\mathcal{W}_3 \equiv \mathcal{W}^{pA}$. The binary potentials generally have a nonlocal dependence on the momentum coordinates p and p' or $\mathcal{W}^{N-A} = \mathcal{W}^{N-A, \mathcal{I}^\pi}_{\nu\nu'}(p, p')$, where ν (ν') represents angular momentum channels and $\mathcal{I}^\pi$ is the spin-parity of the system. For each arrangement channel i, in the center-of-mass (c.m.) frame, the system can be represented by a pair of Jacobi momenta: the relative momentum of the pair ($\vec{p}_i \equiv p_i \, \hat{p}_i$) and the momentum of the spectator with respect to the c.m. of the pair ($\vec{q}_i \equiv q_i \, \hat{q}_i$). As such, the kinetic energy is given by [34]

$$H_0 = \frac{p_i^2}{2\mu_i} + \frac{q_i^2}{2M_i}, \tag{1}$$

where μ_i and M_i are, respectively, the reduced masses for the interacting pair (jk) and for the $i + (jk)$ system, where (i, j, k) form a cyclic permutation of (1,2,3). At the relative three-body energy E, the exact three-body scattering wave function for the incident arrangement channel 1 ($|\Psi_{(1)}\rangle$) fulfills the Schrödinger equation

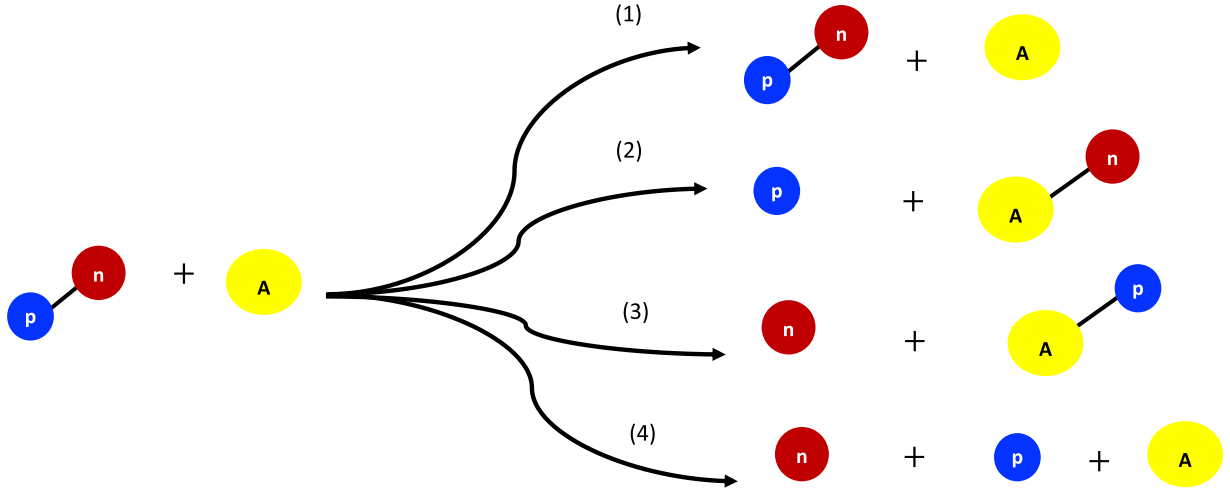$$[E - H_0]|\Psi_{(1)}\rangle = \sum_{i=1}^{3} \mathcal{W}_i |\Psi_{(1)}\rangle. \tag{2}$$

FIG. 1. Schematic representation of all possible three-body rearrangement processes arising from the scattering of a deuteron with a target nucleus A. The arrows (1)–(4) represent elastic scattering, neutron transfer, proton transfer, and three-body breakup.

The asymptotics of the wave function $|\Psi_{(1)}\rangle$ contain information about all possible three-body processes and therefore has complicated boundary conditions that make its direct determination unfeasible. To circumvent this issue, Faddeev [3] introduced the components $|\psi_{i1}\rangle \equiv G_0(E)\,\mathcal{W}_i|\Psi_{(1)}\rangle$ so that the wave function is given by the sum $|\Psi_{(1)}\rangle = |\psi_{11}\rangle + |\psi_{21}\rangle + |\psi_{31}\rangle$, where the free propagator has the definition $G_0(E) = [E - H_0 + i0]^{-1}$. Unlike the full wave function, the asymptotics of each Faddeev component describe a specific reaction channel, in the present case of deuteron-induced reactions $|\psi_{11}\rangle$, $|\psi_{21}\rangle$, and $|\psi_{31}\rangle$ describe elastic deuteron scattering, neutron transfer, and proton transfer reactions, respectively.

Since scattering wave functions are ill behaved in momentum space, it is customary to work with transition operators instead. In the case of three-body scattering the transition operators U^{11}, U^{21}, and U^{31}, contain the same information as the corresponding Faddeev components and fulfill a set of coupled momentum space integral equations [32] (Faddeev-AGS equations)

$$U^{i1}(E) = \bar{\delta}_{i1}\,G_0^{-1}(E) + \sum_{k=1}^{3} \bar{\delta}_{ik}\,t_k(E)\,G_0(E)\,U^{k1}(E). \quad (3)$$

Here, $\bar{\delta}_{ik} \equiv 1 - \delta_{ik}$ is the anti-Kronecker delta and $t_i(E)$ is the binary t matrix given by the Lippmann-Schwinger (LS) equation $t_i(E) = \mathcal{W}_i + \mathcal{W}_i\,G_0(E)\,t_i(E)$. For processes leading to complete three-body breakup the corresponding transition operator is given by $U^{01} = U^{11} + U^{31} + U^{31}$. The transition amplitudes are connected to the scattering matrix (s matrix) through the relation $S^{i1} = \delta_{i1} - 2\pi i\delta(E - H_0)\,U^{i1}$. We proceed by introducing the states $|q_i(\lambda_i I_i^{\pi_i})\mathcal{J}_i M_{\mathcal{J}_i}\rangle$, which describe the motion of the spectator relative to the pair with λ_i and $I_i^{\pi_i}$ representing the orbital angular momentum and spin parity of the spectator, respectively. Here $\mathcal{J}_i$ and $M_{\mathcal{J}_i}$ denote the total spectator angular momentum and its z-axis projection. Additionally, the bound-state wave function of the

pair ($|\phi_{im}^{\mathcal{I}_i^{\pi_i}}\rangle$) is given by the Schrödinger equation

$$\left[\varepsilon_i^{(m)} - \frac{p_i^2}{2\mu_i}\right]|\phi_{im}^{\mathcal{I}_i^{\pi_i}}\rangle = \mathcal{W}_i^{\mathcal{I}_i^{\pi_i}}|\phi_{im}^{\mathcal{I}_i^{\pi_i}}\rangle, \quad (4)$$

where $m = 1 \ldots N_{\text{bound}}$ is an index enumerating the bound states and N_{bound} is the number of bound states. Here $\varepsilon_i^{(m)}$ is the binding energy of the mth bound state and $\mathcal{I}_i^{\pi_i}$ is the spin parity of the pair. The channel state corresponding to an arrangement channel i and a conserved total angular momentum J is constructed by coupling the bound state of the pair to the relative motion of spectator leading to

$$\big|\Phi_{m\alpha_i}^{(i),JM}\big\rangle|q_i\rangle \equiv |q_i\rangle\Big[\big|\phi_{im}^{\mathcal{I}_i^{\pi_i}}\big\rangle|(\lambda_i I_i)\mathcal{J}_i\rangle\Big]^{JM}, \quad (5)$$

where $\alpha_i = \{\mathcal{I}_i^{\pi_i}, \lambda_i, I_i^{\pi_i}, \mathcal{J}_i\}$ and M is the z-axis projection of J. The transition matrix elements needed to evaluate the cross section for the process $1 \longrightarrow i$ are then given by

$$X_{m\alpha_i,n\alpha_1'}^{i1,J}(q_i, q_1'; E) \equiv \langle q_i|\langle\Phi_{m\alpha_i}^{(i),JM}|\,U^{i1}(E)\,\big|\Phi_{n\alpha_1}^{(1),JM}\big\rangle|q_1'\rangle,$$

$$\equiv \big\langle q_i\big|X_{m\alpha_i,n\alpha_1'}^{i1,J}(E)\big|q_1'\big\rangle. \quad (6)$$

For cross section calculations we only need transition matrix elements for which q_{im} and q_{1n}' are determined by the on-shell condition.

To obtain numerical solutions of the Faddeev-AGS equations, we first note that the pairwise potentials have the general form $\mathcal{W}_i = \mathcal{W}_i^{\text{s}} + \bar{V}_i^{\text{c}}$, where $\mathcal{W}_i^{\text{s}}$ is short ranged and $\bar{V}_i^{\text{c}} = Z_j Z_k e^2/r$ is the average Coulomb potential, with $Z_j(Z_k)$ being the charge of particle $j(k)$. The corresponding binary t matrix can be written as $t_i(E) = t_i^{\text{c}}(E) + t_i^{\text{s}}(E)$, where $t_i^{\text{c}}(E)$ is the t matrix associated with the average Coulomb potential and t_i^{s} is the solution of the LS equation using the short-ranged residual interaction $\mathcal{W}_i^{\text{s}} \equiv \mathcal{W}_i - \bar{V}_i^{\text{c}}$ in the basis of Coulomb scattering wave functions. The presence of the term $t_i^{\text{c}}(E)$ introduces nonintegrable singularities in the kernel of Eqs. (3) and thus renders a direct numerical solution unfeasible [32,35]. By subtracting $t_i^{\text{c}}(E)$ from the overall t matrix, one can reformulate

the Faddeev-AGS equations leading to [32]

$$U^{i1}(E) = U^{c,i1}(E) + \sum_{k=1}^{3} U^{c,ik}(E) \, t_k^s(E) \, G_0(E) \, U^{k1}(E), \quad (7)$$

where $U^{c,ik}$ is the solution of the Faddeev-AGS equations with only the average Coulomb potential and has an analytical solution when only two of the three particles are charged. To arrive at a numerical solution for Eqs. (8), we express the short-ranged pairwise potentials in separable form via expansion in a basis $\{|\bar{h}_n^i\rangle\}$ (e.g., Ernst-Shakin-Thaler [36] basis),

$$\mathcal{W}_i^s(E) = \sum_{\beta,\gamma=1}^{N_{\text{rank}}} |\bar{h}_\beta^i\rangle \, \lambda_{i,\beta\gamma}^s \, \langle\bar{h}_\gamma^i|, \quad (8)$$

where N_{rank} is the number of basis functions, which are enumerated by the indices $\beta(\gamma)$ hereafter. This representation for $\mathcal{W}_i^s$ leads to a corresponding separable form of the binary t matrix

$$t_i^s(E) = \sum_{n=1}^{N_{\text{bound}}} |\tilde{h}_n^i\rangle \, g_{in}^0(E) \, \langle\tilde{h}_n^i| + \sum_{\beta\gamma=1}^{N_{\text{rank}}} |\bar{h}_\beta^i\rangle \, \bar{\tau}_{i,\beta\gamma}^s(E) \, \langle\bar{h}_\gamma^i|, \quad (9)$$

where $g_{in}^0(E) = (E - \varepsilon_i^{(n)} - q_i^2/M_i + i0)^{-1}$ is the free propagator for the spectator relative to the bound pair. The vectors $|\tilde{h}_n^i\rangle$ appearing in the first term of Eq. (10) are the so-called bound-state form factors and are given by the product of the pairwise potential and the bound-state wave function or $|\tilde{h}_n^i\rangle \equiv \mathcal{W}_i|\phi_m^{(i)}\rangle$. The matrix elements $\bar{\tau}_{i,\beta\gamma}^s(E)$ are determined by substituting Eqs. (9) and (10) into the LS equation. The separable representation of the binary t matrix enables a reformulation of Eqs. (8) in terms of the transition operators defined by Eq. (7) such that [32]

$$X_{mn}^{ij}(E) = Z_{mn}^{ij}(E) + \sum_{k=1}^{3} \sum_{n'=1}^{N_{\text{bound}}} Z_{mn'}^{ik}(E) \, g_{kn'}^0(E) \, X_{n'n}^{kj}(E)$$

$$+ \sum_{k=1}^{3} \sum_{\beta',\gamma'=1}^{N_{\text{rank}}} Z_{m\beta'}^{ik}(E) \, \bar{\tau}_{k,\beta'\gamma'}^s(E) \, X_{\gamma'n}^{kj}(E), \quad (10)$$

and

$$X_{\beta n}^{ij}(E) = Z_{\beta n}^{ij}(E) + \sum_{k=1}^{3} \sum_{n'=1}^{N_{\text{bound}}} Z_{\beta n'}^{ik}(E) \, g_{kn'}^0(E) \, X_{n'n}^{kj}(E)$$

$$+ \sum_{k=1}^{3} \sum_{\beta',\gamma'=1}^{N_{\text{rank}}} Z_{\beta\beta'}^{ik}(E) \, \bar{\tau}_{k,\beta'\gamma'}^s(E) \, X_{\gamma'n}^{kj}(E), \quad (11)$$

where we have suppressed the channel index α_i for brevity and the second equation is needed to determine the nonphysical transition operators $X_{\gamma'n}^{kj}(E)$. The effective potentials have the definition

$$Z_{nm}^{ij}(E) \equiv \langle\tilde{h}_m^i|G_0(E) \, U^{c,ij}(E) \, G_0(E)|\tilde{h}_n^j\rangle, \quad (12)$$

and their computation is generally very complicated since $U^{c,ij}(E)$ is the transition operator for the scattering of three particles under the exclusive influence of the average Coulomb potential. However, it simplifies immensely for cases where one of the particles is neutral. For example, if particle 3 is neutral the Coulomb three-particle transition operator

reduces to $U^{c,ij}(E) = \bar{\delta}_{ij} \, G_0^{-1}(E) + \bar{\delta}_{i3} \, t_3^c(E)$, where $t_3^c(E)$ is the two-body Coulomb scattering t matrix for particles 2 and 3. The effective potentials can be numerically evaluated using

$$Z_{mn}^{ij}(E) \equiv \bar{\delta}_{ij} \, \langle h_m^i| \, G_0(E) \, |h_n^j\rangle + \bar{\delta}_{i3} \, \bar{\delta}_{j3} \, \langle h_m^i| \, G_0(E)$$

$$\times t_3^c(E) \, G_0(E) \, |h_n^j\rangle. \quad (13)$$

It was already shown in Ref. [37] that the momentum space matrix elements of the diagonal effective potentials $\langle\vec{q}_i'|Z_{mn}^{ii}|\vec{q}_i\rangle$ contain a singularity in the forward direction $(\vec{q}_i \longrightarrow \vec{q}_i')$. The nature of the singularity is revealed by replacing the Coulomb t matrix with its Born approximation $t_3^c = \bar{V}_3^c$, leading to the factorization of the matrix elements $\langle\vec{q}_i'|Z_{mn}^{ii}|\vec{q}_i\rangle = \bar{\delta}_{i3} \, \langle h_m^i| \, G_0(E, q_i') \, G_0(E, q_i) \, |h_n^i\rangle \times \bar{V}_3^c(|\vec{q}_i' - \vec{q}_i|)$. The forward singularity of the average Coulomb potential is thus propagated into the diagonal effective potentials, leading to nonintegrable singularities in the kernels of Eqs. (12) and (14). To circumvent this challenge, the Born term is subtracted and treated analytically according to the Gell-Mann-Goldberger [38] relation (two-potential formula). Specifically, one defines the regularized effective potentials

$$Z_{mn}^{sc,ij} = Z_{mn}^{ij} - \bar{V}_3^c \, \delta_{ij} \, \delta_{mn}, \quad (14)$$

so that the full transition operator is given by the sum $X_{mn}^{ij} = X_{mm}^{c,ii} \, \delta_{mn} + \Omega_{im}^c \, X_{mn}^{sc,ij} \, \Omega_{jn}^c$, where $X_{mm}^{c,ii}$ corresponds to the Rutherford scattering amplitude, $\Omega_{im}^c(E) \equiv g_{im}^c(E) \, g_{im}^{0,-1}(E)$ is the Möller wave operator with $g_{im}^c(E) = (E - \varepsilon_i^{(m)} - q_i^2/M_i - \bar{V}_i^c + i0)^{-1}$ being the Coulomb propagator. The regularized transition operators $X_{mn}^{sc,ij}$ are free of singularities and are obtained by solving the modified Faddeev-AGS equations [32],

$$X_{mn}^{sc,ij}(E) = Z_{mn}^{sc,ij}(E) + \sum_{k=1}^{3} \sum_{n'=1}^{N_{\text{bound}}} Z_{mn'}^{sc,ik}(E) \, g_{kn'}^c(E) \, X_{n'n}^{sc,kj}(E)$$

$$+ \sum_{k=1}^{3} \sum_{\beta',\gamma'=1}^{N_{\text{rank}}} Z_{m\beta'}^{sc,ik}(E) \, \bar{\tau}_{k,\beta'\gamma'}^{sc}(E) \, X_{\gamma'n}^{sc,kj}(E), \quad (15)$$

and

$$X_{\beta n}^{sc,ij}(E) = Z_{\beta n}^{sc,ij}(E) + \sum_{k=1}^{3} \sum_{n'=1}^{N_{\text{bound}}} Z_{\beta n'}^{sc,ik}(E) \, g_{kn'}^c(E) \, X_{n'n}^{sc,kj}(E)$$

$$+ \sum_{k=1}^{3} \sum_{\beta',\gamma'=1}^{N_{\text{rank}}} Z_{\beta\beta'}^{sc,ik}(E) \, \bar{\tau}_{k,\beta'\gamma'}^{sc}(E) \, X_{\gamma'n}^{sc,kj}(E). \quad (16)$$

In this work we diagonalize Eqs. (19) and (21) in a Coulomb basis to arrive at the transition amplitudes $X_{mn}^{ij}(q_i, q_j)$ needed to evaluate cross sections for the various three-body processes. A detailed discussion on the evaluation of the effective potentials $Z_{mn}^{sc,ij}(E)$ and the diagonalization of the resulting Faddeev-AGS equations in the Coulomb basis can be found in Ref. [31].

B. Microscopic calculation of nucleon-nucleus potentials in momentum space

The ingredients for the three-body Faddeev calculations discussed in Sec. II A are the momentum space microscopic

pairwise N-A potentials ($\mathcal{W}_{NA}$) in addition to the n-p interaction. To compute $\mathcal{W}_{NA}$, we start from the microscopic $(A + 1)$-body Hamiltonian, which in general includes two- and three-nucleon (NN and 3N) forces,

$$H = \sum_{i<j=2}^{A+1} \frac{(\vec{k}_i - \vec{k}_j)^2}{2m_N} + \sum_{i<j=2}^{A+1} V_{ij}^{\mathrm{NN}} + \sum_{i<j<k=3}^{A+1} V_{ijk}^{\mathrm{3N}}, \quad (17)$$

where $\vec{k}_i$ is the momentum of the ith nucleon and m_N is the nucleon mass. The many-body Hamiltonian can be recast as

$$H = H^{(A)} + \frac{p^2}{2\mu} + \bar{V}^{\mathrm{c}}(r) + V^{\mathrm{rel}}, \quad (18)$$

where the intrinsic Hamiltonian $H^{(A)}$ governs the dynamics of the A-nucleon target within the $N + A$ system, with p and μ being the relative momentum and reduced mass of the $N + A$ system. Here $\bar{V}^{\mathrm{c}}(r) = \frac{1}{2}(1 + \tau_{A+1}^z)Ze^2/r$ is the average N-A Coulomb potential (with Z and τ_{A+1}^z representing, respectively, the atomic number of the target and twice the isospin projection of the nucleon), and the relative nucleon-nucleus interaction is given by

$$V^{\mathrm{rel}} = \sum_{i=1}^{A} V_{i,A+1}^{\mathrm{NN}} + \sum_{i<j=2}^{A} V_{ij,A+1}^{\mathrm{3N}} - \bar{V}^{\mathrm{c}}(r). \quad (19)$$

In momentum space, the NCSM/RGM ansatz [28] for the $N + A$ scattering wave function for a given spin-parity and isospin ($\mathcal{I}^\pi T$) takes the form

$$\left| \Psi_{\nu_0; p_0}^{\mathcal{I}^\pi T} \right\rangle = \sum_\nu \int dp\, p^2\, \chi_{\nu\nu_0}^{\mathcal{I}^\pi T}(p, p_0)\, \mathcal{A}_\nu \left| \Phi_{\nu p}^{\mathcal{I}^\pi T} \right\rangle, \quad (20)$$

where ν is a collective index denoting an arbitrary angular momentum channel while ν_0 and p_0 indicate the incident channel and momentum. If we chose I_A, π_A, T_A, and α_A to denote, respectively, the spin, parity, isospin, and additional quantum numbers of the target nucleus, the channel states are given by

$$\left| \Phi_{\nu p}^{\mathcal{I}^\pi T} \right\rangle = \left[\left(\left| A\, \alpha_A I^{\pi_A} T_A \right\rangle \left| 1\, \frac{1}{2}^{+}\, \frac{1}{2} \right\rangle \right)^{sT} Y_\ell(\hat{p}_{A,A+1}) \right]^{\mathcal{I}^\pi T}$$
$$\times \frac{\delta(p - p_{A,A+1})}{p\, p_{A,A+1}}, \quad (21)$$

where $| \alpha_A I^{\pi_A} T_A \rangle$ is an eigenstate of the intrinsic Hamiltonian $H^{(A)}$ with energy eigenvalue $E_\nu^{(A)}$, s the total spin, and ℓ the relative orbital angular momentum for the $N + A$ system in channel ν. The eiegenstate is obtained by diagonalizing $H^{(A)}$ in the model space spanned by the NCSM $N_{\mathrm{max}}\hbar\Omega$ harmonic oscillator (HO) basis. Here N_{max} is the maximum number of HO quanta above the minimum energy configuration of the nucleons and Ω is the HO frequency. The operator $\mathcal{A}_\nu$ antisymmetrizes the incident nucleon with respect to the nucleons in the target A. The angular motion of the projectile nucleon with respect to the target nucleus is described by $Y_\ell(\hat{p}_{A,A+1})$ while the relative momentum is given by

$$\vec{p}_{A,A+1} = p_{A,A+1}\, \hat{p}_{A,A+1} = \frac{A}{A+1} \left[\vec{k}_{A+1} - \frac{1}{A} \sum_{i=1}^{A} \vec{k}_i \right]. \quad (22)$$

By introducing the momentum-space norm $\mathcal{N}_{\nu\nu'}^{\mathcal{I}^\pi T}(p, p') \equiv \langle \Phi_{\nu p}^{\mathcal{I}^\pi T} | \mathcal{A}_\nu \mathcal{A}_\nu' | \Phi_{\nu' p'}^{\mathcal{I}^\pi T} \rangle$ and adopting the orthogonalization procedure of Ref. [28], the $(A + 1)$-body Schrödinger equation can be reduced into the binary form

$$\left[E_{A+1} - E_\nu^{(A)} - \frac{p^2}{2\mu} \right] \chi_{\nu\nu_0}^{\mathcal{I}^\pi T}(p, p_0)$$
$$= \sum_{\nu'} \int dp'\, p'^2\, \mathcal{W}_{\nu\nu'}^{\mathcal{I}^\pi T}(p, p')\, \chi_{\nu'\nu_0}^{\mathcal{I}^\pi T}(p', p_0), \quad (23)$$

where $\chi_{\nu'\nu_0}^{\mathcal{I}^\pi T}(p', p_0)$ is the amplitude of relative motion, $\mathcal{W}_{\nu\nu'}^{\mathcal{I}^\pi T}(p, p')$ the effective two-body N-A potential and E_{A+1} the total energy of the $N + A$ system. The N-A potential

$$\mathcal{W}_{\nu\nu'}(p, p') = \bar{\mathcal{H}}_{\nu\nu'}^{\mathrm{mod}}(p, p') + \mathcal{W}_{\nu\nu'}^{\mathrm{eey}}(p, p') + \mathcal{W}_{\nu\nu'}^{\mathrm{kin}}(p, p')$$
$$+ \bar{\mathcal{V}}_{\nu\nu'}^{\mathrm{coul}}(p, p'), \quad (24)$$

contains contributions from: i) the orthogonalized Hamiltonian kernel inside the HO model space ($\bar{\mathcal{H}}_{\nu\nu'}^{\mathrm{mod}}$), ii) the energy eigenvalue of the target nucleus ($\mathcal{W}_{\nu\nu'}^{\mathrm{eey}}$), iii) the relative kinetic energy ($\mathcal{W}_{\nu\nu'}^{\mathrm{kin}}$), and iv) the average Coulomb potential ($\bar{\mathcal{V}}_{\nu\nu'}^{\mathrm{coul}}$), where we have dropped the $J^\pi T$ superscript for brevity. Details of the derivation of the expressions for $\mathcal{W}_{\nu\nu'}^{\mathcal{I}^\pi T}(p, p')$ are presented in Appendix.

The corresponding t matrix that serves as input to the Faddeev-AGS equations and is needed for computing $N + A$ scattering phase shifts satisfies the momentum space Lippmann-Schwinger (LS) equation

$$t_{\nu\nu_0}^{\mathcal{I}^\pi T}(p, p_0; E_{\mathrm{kin}}) = \mathcal{W}_{\nu\nu_0}^{\mathcal{I}^\pi T}(p, p_0) + \sum_{\nu'} \int dp'\, p'^2$$
$$\times \mathcal{W}_{\nu\nu'}^{\mathcal{I}^\pi T}(p, p')\, G_{0\nu}(E_{\mathrm{kin}}, p')\, t_{\nu\nu_0}^{\mathcal{I}^\pi T}$$
$$\times (p', p_0; E_{\mathrm{kin}}), \quad (25)$$

which is equivalent to Eq. (23) complemented by the scattering boundary conditions, and the propagator is given by $G_{0\nu}(E_{\mathrm{kin}}, p') = [E_{\mathrm{kin}} - \epsilon_\nu - p'^2/2\mu + i0]^{-1}$. Here $E_{\mathrm{kin}} \equiv E_{A+1} - E_{\nu_0}^{(A)}$ is the relative kinetic energy of $N + A$ system corresponding to the incident channel while $\epsilon_\nu \equiv E_\nu^{(A)} - E_{\nu_0}^{(A)}$ is the excitation energy of the target nucleus. As already noted in Sec. II A, the Faddeev calculations require a separable representation of the short-ranged component of the potential $\mathcal{W}_{\nu\nu'}^{\mathcal{I}^\pi T}(p, p')$. This is achieved by applying the Ersnt-Shakin-Thaler [36,39] (EST) scheme, which has been extensively verified for both nucleon-nucleus [40–42] and deuteron-nucleus systems [34,43]. We also note that, unlike typical phenomenological potentials based on local Woods-Saxon (WS) functions, microscopic NCSM/RGM pairwise potentials employed in this work are intrinsically separable because they are given by expansions in the radial wave functions for p and p' separately. The EST scheme is merely employed to arrive at a specific separable form for $\mathcal{W}_{\nu\nu'}(p, p')$ that is convenient for solving the Faddeev-AGS equations and an accurate representation is attained using a small basis size.
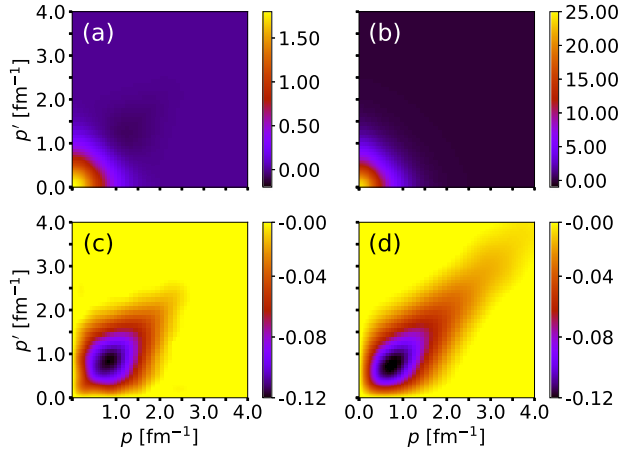
FIG. 2. The partial wave n-α potential $W_l^{\mathcal{I}}(p, p')$ in units of fm^2 as a function of the momenta p and p'. (a) and (c) depict, respectively, the $s_{1/2}$ and $p_{3/2}$ microscopic NCSM/RGM potentials while the corresponding Woods-Saxon (WS) potential is shown in (b) and (d), respectively. The WS potential is scaled down by the strength of the Pauli projector [34] $\Gamma = 1100$ fm^{-1}. The NCSM/RGM model space is truncated at $N_{\max} = 12/13$ for the positive/negative parity partial waves with $\hbar\Omega = 14$ MeV and $\lambda_{\rm SRG} = 1.5$ fm^{-1}.

III. RESULTS AND DISCUSSION

A. Momentum-space microscopic $n +{}^4$He and $p +{}^4$He potentials

The starting point for all our calculations is a soft SRG-evolved NN potential at fourth order (SRG-N³LO NN potential) obtained by evolving the χEFT interaction of Ref. [9] to a momentum resolution scale of $\lambda_{\rm SRG} = 1.5$ fm^{-1}. The low momentum resolution scale helps to speed up convergence of the HO expansion and ensures a reasonable description of ⁶Li bound state properties despite the omission of explicit 3N forces. For all calculations presented in this section the wave function of the α particle is evaluated using an HO basis expansion up to $N_{\max} = 12$ while the positive/negative-parity NCSM/RGM partial-wave potentials are computed in momentum space using $N_{\max} = 12/13$ for the N-α system. This model space, together with the HO frequency $\hbar\Omega = 14$ MeV, was demonstrated to yield an accurate convergence for the d-α phase shifts for an identical choice of the NN interaction [47].

To obtain the microscopic N-α momentum-space potentials required as input for the Faddeev $n + p + \alpha$ calculation, we apply the momentum-space NCSM/RGM approach described in Sec. II B. For this case, the N-α potentials are diagonal in ℓ and the isospin is fixed at $T = 1/2$, or $\mathcal{W}_{\nu\nu'}^{\mathcal{I}^\pi T} \equiv W_\ell^{\mathcal{I}} \delta_{\nu\nu'}$, since the ground state spin and isospin of the α particle are zero. First, we note that the NCSM/RGM-generated N-α potentials are smooth short-ranged functions of the momentum coordinates (Fig. 2) and are therefore suitable for implementation in the Faddeev-AGS framework to compute $d + \alpha$ observables. Further, we see that the microscopically computed p-wave potential (Fig. 3) has a similar shape to the phenomenologically fitted Woods-Saxon (WS) potential [44] at low momenta. However, there is a bigger difference
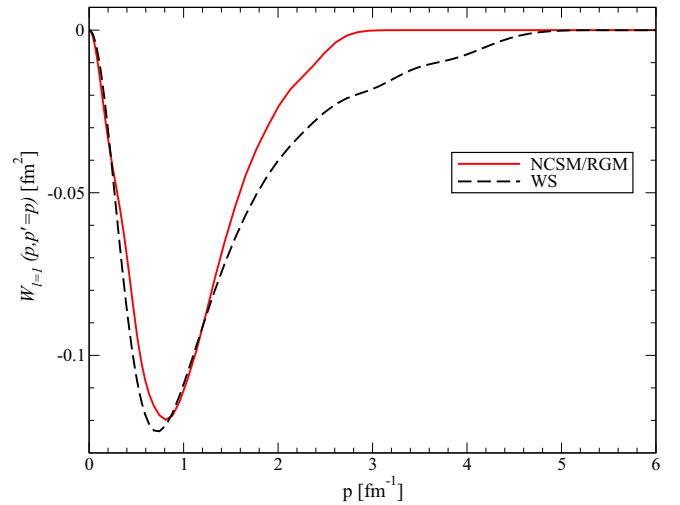

FIG. 3. The diagonal elements of the p-wave potential $W_{\ell=1}^{\mathcal{I}}(p, p' = p)$ for the $n + \alpha$ system as a function of the relative momentum coordinate p. The (red) solid lines depicts the microscopic potentials computed with the NCSM/RGM while the corresponding Woods-Saxon (WS) phenomenological potential [44] is indicated by the (black) dashed line. The NCSM/RGM model space is truncated at $N_{\max} = 13$ with $\hbar\Omega = 14$ MeV and $\lambda_{\rm SRG} = 1.5$ fm^{-1}.

at large momenta owing to the presence of high-momentum components in the WS potential. A comparison for the s wave (Fig. 4) shows that the shape of the microscopically computed potentials is similar to its WS counterpart. Similarly to the p-wave potential, the s-wave potential NCSM/RGM
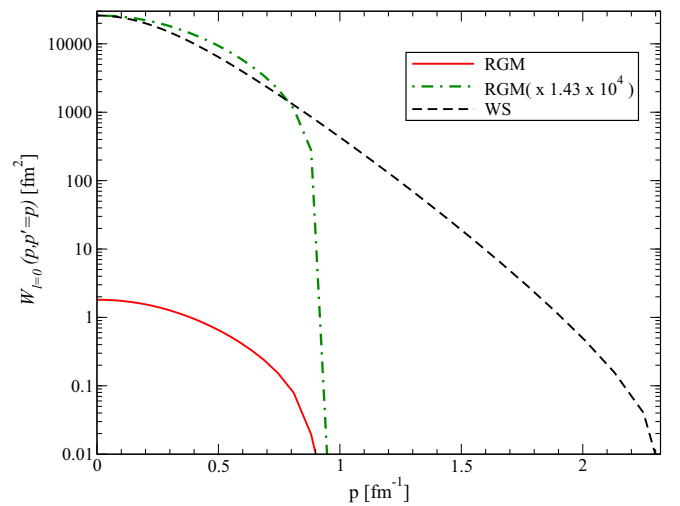

FIG. 4. The diagonal elements of the $s_{1/2}$ potential $W_{\ell=0}^{\mathcal{I}}(p, p' = p)$ for the $n + \alpha$ system as a function of the relative momentum coordinate p. The microscopic potentials computed with the NCSM/RGM are depicted by (red) solid lines while the Woods-Saxon (WS) phenomenological potentials [44] are indicated by (black) dashed lines. A scaled up (by a factor of 1.43×10^4) NSM/RGM potential is indicated by the (green) dash-dotted line. The NCSM/RGM model space is truncated at $N_{\max} = 12$ with $\hbar\Omega = 14$ MeV and $\lambda_{\rm SRG} = 1.5$ fm^{-1}.
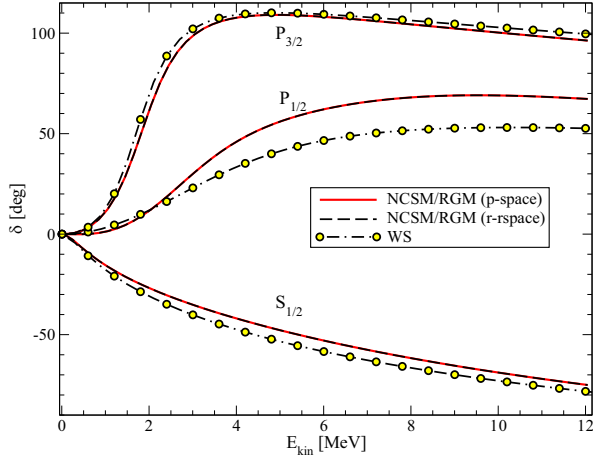
FIG. 5. The phase shifts for $n + \alpha$ scattering as a function of the relative kinetic energy. The (red) solid lines show the phase shifts computed in momentum space using the LS equation while the (black) dashed lines represent the corresponding coordinate space results obtained via the microscopic R-matrix formalism [45,46]. The dash-dotted lines with circles indicate the phase shifts computed using a phenomenologically fitted Woods-Saxon (WS) potential [44]. The NCSM/RGM model space is truncated at $N_{\max} = 12/13$ for the positive/negative parity partial waves. Note that the coordinate space and momentum space NCSM/RGM results are indistinguishable within the line thickness.

potential lacks the high-momentum components owing to the low-momentum resolution of the NN potential used in the microscopic calculation. We also note that the magnitude of the WS s-wave potential is orders of magnitude larger than the NCSM/RGM potential. This is a consequence of the approximate treatment of the Pauli exclusion principle in the WS potential [34]. Specifically, the WS well used to fit the $N + \alpha$ phase shifts supports a Pauli-forbidden bound state that is removed by adding the term $|\phi_0\rangle \Gamma \langle\phi_0|$, with $|\phi_0\rangle$ being the bound-state wave function and the parameter $\Gamma \to \infty$ is the strength of the Pauli projector (in practice we work with finite values, e.g., $\Gamma = 1100$ fm^{-1} in this case). This procedure approximates the Pauli exclusion principle by effectively shifting the spurious bound state to very large positive energies, well beyond the kinematic range under consideration, leading to the unusually large values for the s-wave potential. It should be pointed out that, since the magnitude of the s-wave potential reflects the size of the projector strength, it is arbitrarily large. Also, the scattering states are unaffected by the projector term so that the phase shifts are identical to those of the unmodified Woods-Saxon potential.

To verify the accuracy of the NCSM/RGM-generated momentum space potentials, we employ the LS equation (25) to compute N-α scattering phase shifts and compare them with the results obtained by solving the orthogonalized NCSM/RGM equations in coordinate space, using the microscopic R-matrix method on a Lagrange mesh [45,46]. The agreement between the two calculations is excellent (Fig. 5), and demonstrates the accuracy of the momentum space N-α potentials. We also compare the results of the microscopic potentials to the phase shifts computed using the phenomeno-

logical WS fits. There is generally a reasonable agreement for the $s_{1/2}$ and $p_{3/2}$ partial waves. The $s_{1/2}$ phase shifts are substantially larger than those of the WS potential, indicating an underestimation of the spin-orbit splitting, as already observed in Ref. [47]. The inclusion of three-nucleon forces combined with the solution of the problem within the more complete approach of the no-core shell model with continuum (NSCMC) resolves this issue [48,49].

B. NCSM/RGM calculations for ^{6}Li and d-^{4}He scattering

We obtain the fully microscopic solution for the d-α bound and scattering states using the NCSM/RGM approach for deuteron-nucleus systems [47]. To enable a direct comparison with the Faddeev $n + p + \alpha$ calculations, we employ the same NN interaction and consistent HO model space as for the N-α potentials (Sec. III A). Different from the Faddeev formalism, here the wave function of the deuteron projectile is computed by diagonalizing the two-nucleon intrinsic Hamiltonian in a two-body NCSM model space of consistent size $N_{\max}$ and HO frequency Ω as the α particle. Further, the deformation and virtual breakup of the weakly bound deuteron projectile are treated by including excited deuteron pseudostates (discretizing the deuteron continuum) in the NCSM/RGM coupled-channel equations, similar to what was done in Ref. [47]. In that work it was demonstrated that the inclusion of the $n + p$ angular momentum channels $^3S_1 - {}^3D_1$, $^3D_2$, and $^3D_3 - {}^3G_3$, while limiting the number of deuteron pseudostates to no more than seven, yields well-converged results for the $d + \alpha$ system.

C. Faddeev calculations for the $d + {}^4$He system

We proceed to solve the bound-state Faddeev equations for the $n + p + \alpha$ system using the effective three-body Hamiltonian of Eq. (1) where $\mathcal{W}_{n\alpha}$, and $\mathcal{W}_{p\alpha}$ are computed microscopically as described in Sec. III A, and V^{np} is the same SRG-evolved NN interaction employed in the NCM/RGM calculations above. By varying the value of $N_{\max}$ used in the computation of the $N - \alpha$ potentials, we determine that the ^{6}Li ground-state energy is indeed well converged at $N_{\max} = 12$ (Fig. 6), which is consistent with the convergence patterns of the $d + \alpha$ microscopic calculations discussed in Sec. III B. Additionally, the convergence of the ^{6}Li ground-state energy with $N_{\max}$ is similar to that of the relative binding energies $E_2 \equiv E(^6\text{Li}) - E(\alpha) - E(d)$ and $E_3 \equiv E(^6\text{Li}) - E(\alpha)$. Further, the Faddeev calculation requires a truncation in the number of N-α partial waves included in the effective three-body Hamiltonian. We find that the ^{6}Li ground state is well converged for the total angular momenta $\mathcal{I}_{n+p} \leqslant 3$ and $\mathcal{I}_{N-\alpha} \leqslant 5/2$ for the $n + p$ and $N + \alpha$ subsystems, respectively. The $n + p + \alpha$ three-body binding energy is determined to be $E_3 = -3.18$ MeV, which is combined with the energy of the α particle (Table I) to obtain a ^{6}Li ground-state energy of $E_6 = -31.41$ MeV. The resulting ^{6}Li ground-state energy is found to be $E_6 = -32.01$ MeV, which is approximately 600 KeV more bound than the Faddeev three-body calculation. This underbinding of the Faddeev calculation indicates a missing attractive strength in the
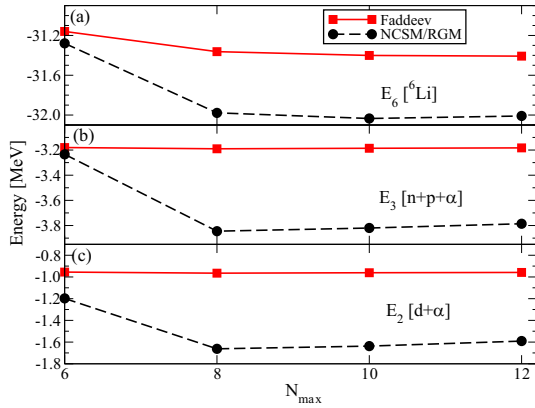
FIG. 6. The ^{6}Li ground-state binding energy as a function of N_{max} calculated using the NCSM/RGM and the three-body Fadeev approach. (a) depicts the total six-body binding energy of ^{6}Li while (b) and (c), respectively, show the relative binding energy for the $n + p + \alpha$ and $d + \alpha$ systems. The Faddeev results are indicated by (red) solid lines with filled squares while the NCSM/RGM calculations are depicted by (black) dashed lines with circles. The NCSM/RGM model space is truncated at $N_{max} = 12/13$ for the positive/negative parity partial waves and $\hbar\Omega = 14$ MeV. The microscopic N-α potentials that was used as input in the Faddeev computation of the ^{6}Li bound state were obtained using $N_{max} = 12/13$ with the angular momentum truncation $\mathcal{I}_{n+p} \leqslant 2$ and $\mathcal{I}_{N+\alpha} \leqslant 5/2$.

$n - p - \alpha$ interaction that is not captured by the sum of the pairwise $n - \alpha$ and $p - \alpha$ potentials. Since the α particle is fixed in its ground state in both the NCSM/RGM and Faddeev calculations, this effect can be attributed to the antisymmetrization of the six nucleon problem. Indeed, a close inspection of the NCSM/RGM deuteron-nucleus potential (see, e.g., Eqs. (B2a)– (B2f) of Ref. [47]) reveals the presence of irreducible three-body terms that arise from a simultaneous exchange of the two nucleons inside the deuteron with nucleons in the α particle.

Next, we solve the Faddeev-AGS equations for $d + \alpha$ scattering at energies below the deuteron breakup threshold, starting from the same three-body Hamiltonian as in the

TABLE I. The ground-state energies for the d, α, and ^{6}Li computed using the SRG-N^{3}LO potential [9] with $\lambda_{SRG} = 1.5$ fm^{-1}. The NCSM results were obtained using $N_{max} = 12$. The binding energy of the deuteron calculated by solving the bound-state LS equation in momentum space for the np system is also listed. The angular momentum channels $^3S_1 - {}^3D_1$, $^3D_2$, and $^3D_3 - {}^3G_3$ of the np system were included in the NCSM/RGM calculation while limiting the number of deuteron pseudostates to no more than seven. The microscopic N-α potentials that was used as input in the Faddeev computation of the ^{6}Li bound state were obtained using $N_{max} = 12/13$ with the angular momentum truncation $\mathcal{I}_{n+p} \leqslant 2$ and $\mathcal{I}_{N+\alpha} \leqslant 5/2$.

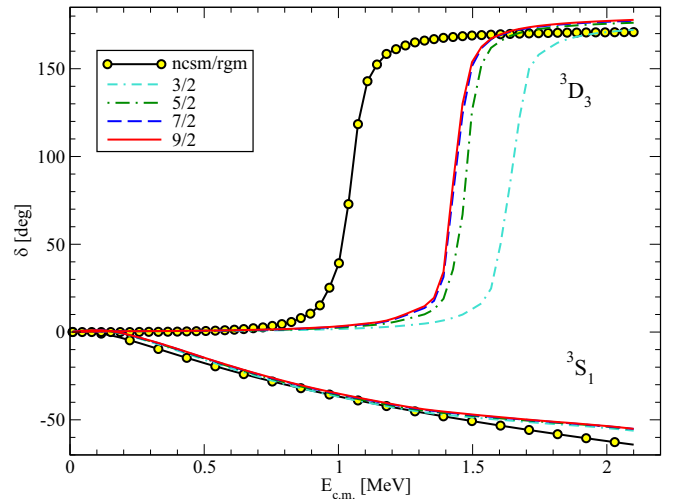|	α (NCSM)	d (NCSM)	d (LS)	^{6}Li (NCSM/RGM)	^{6}Li (Faddeev)
E (MeV)	−28.22	−2.20	−2.22	−32.01	−31.41

FIG. 7. The phase shifts for elastic $d + \alpha$ scattering as a function of the center-of-mass energy for different partial wave three-body model spaces. The (black) solid line with filled circles shows phase shifts computed using the NCSM/RGM. The Faddeev results are depicted by (red) solid, (blue) dashed, (green) dash-dotted, and (turquoise) dash-dash-dotted lines for the partial wave model spaces $\mathcal{I}_{N+\alpha} \leqslant 9/2$, $\mathcal{I}_{N+\alpha} \leqslant 7/2$, $\mathcal{I}_{N+\alpha} \leqslant 5/2$, and $\mathcal{I}_{N+\alpha} \leqslant 3/2$ as indicated in the figure. The $n + p$ partial waves are limited to $\mathcal{I}_{n+p} \leqslant 3$. The NCSM/RGM model space is truncated at $N_{max} = 12/13$ for the positive/negative parity partial waves and $\hbar\Omega = 14$ MeV.

bound-state calculations above. We first illustrate the convergence of the Faddeev calculations with respect to the number $n + p$ and $N + \alpha$ partial waves, and determine that a maximum angular momentum of $\mathcal{I}_{n+p} = 3$ and $\mathcal{I}_{N-\alpha} = 9/2$ is sufficient to reach convergence, respectively (Fig. 7). At the same time, we employ the NCSM/RGM to microscopically compute $d + \alpha$ (g.s) elastic scattering and proceed to compare the results with the Faddeev calculations for the two dominant $d + \alpha$ (g.s) partial waves at these energies. We find that there is a relatively small difference between the $^3S_1$ phase shifts computed using the Faddeev and NCSM/RGM methods. However, there is a significant difference in the $^3D_3$ phase shifts, which manifests primarily as a shift in the position of the 3^+ resonance. The Faddeev calculations yield a resonance energy that is approximately 400 keV larger relative to the NCSM/RGM result, which is consistent with the underbinding observed in the aforementioned ground-state calculations of ^{6}Li. We note that the $^3D_2$ resonance is also shifted higher in energy and lies beyond the kinematic range considered in this work. Lastly, we compute energy and angular distributions in order to quantify the effects of the irreducible three-body force at the level of scattering observables. The energy distributions are dominated by the $^3D_3$ resonance and, as expected, the Faddeev calculation exhibits a peak that is approximately 400 keV higher than that of the NCSM/RGM (Fig. 8). Also, the differences between the angular distributions (Fig. 9) are largest for energies closest to the resonance. The effect of the omitted 3BF arising due to Pauli effects is thus sizable for both the bound state and scattering observables of the $d + \alpha$ system. Moreover, this missing 3BF is attractive in the $d + \alpha$
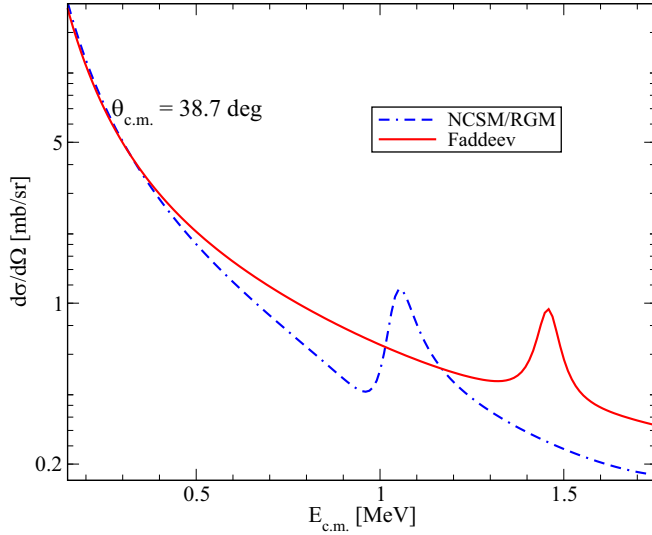
FIG. 8. The differential cross section for elastic $d + \alpha$ scattering as a function of the center-of-mass energy $E_{\text{c.m.}}$ at the scattering angle $\theta_{\text{c.m.}} = 38.7$ deg. The [blue] dashed lines shows phase shifts computed using the NCSM/RGM while the Faddeev results are depicted by (red) solid lines. The model space for the Faddeev calculation is restricted to a total two-body angular momentum of $\mathcal{I}_{n+p} \leqslant 3$ and $\mathcal{I}_{N+\alpha} \leqslant 9/2$ for the $n + p$ and N-α subsystems. The NCSM/RGM model space is truncated at $N_{\max} = 12/13$ for the positive/negative parity partial waves and $\hbar\Omega = 14$ MeV.
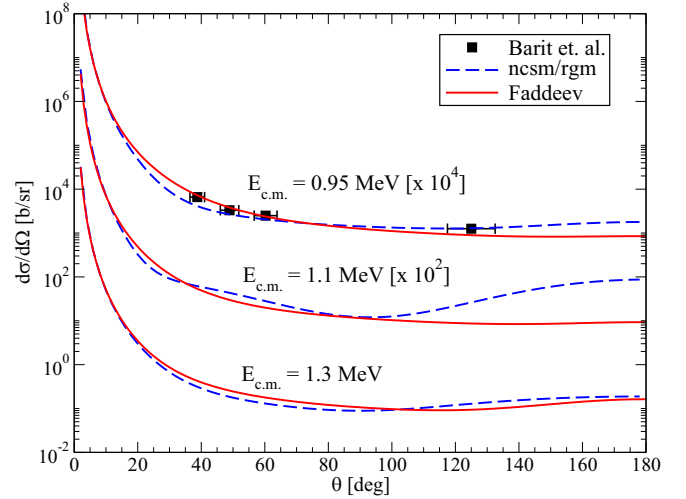

FIG. 9. The differential cross section for elastic $d + \alpha$ scattering as a function of the center-of-mass angle $\theta_{c.m.}$ at varying energies $E_{c.m.}$. The solid lines shows phase shifts computed using the Faddeev method while the NCSM/RGM results are depicted by dashed lines. The model space for the Faddeev calculation is restricted to a total two-body angular momentum of $\mathcal{I}_{np} \leqslant 3$ and $\mathcal{I}_{N-\alpha} \leqslant 9/2$ for the np and N-α subsystems. Experimental data from Ref. [50] are included. The NCSM/RGM model space is truncated at $N_{\max} = 12/13$ for the positive/negative parity partial waves and $\hbar\Omega = 14$ MeV.

partial waves considered here. Since the shapes of angular distributions, e.g., in transfer reactions, are used to extract spectroscopic information, the quality of such information can be impacted by the 3BF effects.

IV. CONCLUSION AND OUTLOOK

While the three-body model provides an indispensable tool for the description of deuteron-induced nuclear reactions, its predictive power is still limited by the lack of constraints on the effective three-body Hamiltonian. Particularly, the reduction of the many-body deuteron-nucleus problem into the three-body space results in an effective Hamiltonian that consists of an irreducible neutron-proton-nucleus 3BF in addition to the pairwise nucleon-nucleus potentials. In this work we have studied the irreducible n-p-α 3BF arising from antisymmetrization effects and quantified its impact on observables of the $d + \alpha$ system. We started from a microscopic five-body Hamiltonian constructed using SRG-evolved N³LO chiral NN potentials and employed the NCSM/RGM [28] to compute momentum space $N + \alpha$ potentials. To benchmark the potentials, we used the LS equation to obtain the corresponding scattering solutions and demonstrated that the resulting phase shifts are in excellent agreement with those obtained via the standard two-body NCSM/RGM by solving R-matrix equations in coordinate space. Next, we constructed an effective three-body potential for the $n + p + \alpha$ system by summing the pairwise potentials and proceeded to solve the corresponding Faddeev-AGS equations for the ⁶Li ground state as well as d-α scattering. At the same time, we carried out correspond-

ing microscopic calculations using the NCSM/RGM starting from a six-body microscopic Hamiltonian based on the same NN interaction as in the $N + \alpha$ case.

We observed that the Faddeev calculation yields a ⁶Li ground state that is approximately 600 keV shallower than the one obtained with the NCSM/RGM, indicating an omitted attractive 3BF. This is consistent with the findings of Ref. [25], where similar calculations based on phenomenological microscopic Hamiltonians were carried out. Additionally, the $d + \alpha$ three-body calculations yield a 3⁺ resonance energy that is approximately 400 keV larger compared to the NCSM/RGM result, which is consistent with the observed underbinding of the ⁶Li ground state. The two methods also yield angular distributions with different shapes due to differences in the position of the 3⁺ resonance. Since the α particle is fixed in its ground state, the origin of this 3BF can be ascribed to two-nucleon exchange processes that are intrinsically three-body in nature.

In the future, three-body calculations of $d + \alpha$ may be improved by using the two-nucleon exchange terms in NCSM/RGM-generated $d - \alpha$ potential to evaluate the irreducible three-body force. Moreover, a similar study based on more complete formalism of the NCSMC [48,51] [where the NCSM/RGM ansatz is augmented with an expansion in square-integrable NCSM eigenstates of the composite ($A +$ 2)-nucleon system], is necessary for the quantification of additional components arising from excitations of the nucleons inside the target nucleus. Lastly, performing similar studies for other light nuclei and establishing a mass dependence of the irreducible three-body force would provide valuable

information for phenomenological models that have a wider range of applicability in mass and energy.

APPENDIX: *AB INITIO* NUCLEON-NUCLEUS POTENTIALS IN MOMENTUM SPACE

To compute the potential $\mathcal{W}_{\nu\nu'}^{\mathcal{I}^\pi T}(p', p)$, we first note that the norm kernel consists of the identity operator and a short-ranged exchange term $\mathcal{N}_{\nu\nu'}^{\mathrm{ex},\,\mathcal{I}^\pi T}(p', p)$, so that $\mathcal{N}_{\nu\nu'}^{\mathcal{I}^\pi T}(p, p') = \delta_{\nu\nu'}\frac{\delta(p-p')}{pp'} + \mathcal{N}_{\nu\nu'}^{\mathrm{ex},\,\mathcal{I}^\pi T}(p', p)$. The superscript $\mathcal{I}^\pi T$ will be dropped from all terms hereafter for brevity. We proceed by defining the harmonic oscillator (HO) model space

$$P_\ell \equiv \sum_{n=0}^{n_{\max}} |R_{n\ell}\rangle\langle|R_{n\ell}|, \tag{A1}$$

and the complimentary space $Q_\ell \equiv 1 - P_\ell$, where the basis vectors are the radial harmonic oscillator wave functions $|R_{n\ell}\rangle$, with n being the radial quantum number. The second term of the norm kernel can be accurately represented within the model space P, owing to its short-ranged character. Contrarily, the δ function has components within the HO model space as well as in the complimentary space. By defining the component of the norm kernel inside the model space $\Lambda_{n\nu,n'\nu'}$, we can express the momentum space norm kernel in the form

$$\mathcal{N}_{\nu\nu'}(p, p') = \delta_{\nu\nu'} Q_\ell(p, p') + [P \Lambda P]_{\nu\nu'}(p', p),$$

$$\equiv \left[\frac{\delta(p-p')}{pp'} - \sum_n \tilde{R}_{n\ell}(p)\tilde{R}_{n\ell}(p')\right]\delta_{\nu\nu'}$$

$$+ \sum_{nn'} \tilde{R}_{n\ell}(p) \Lambda_{n\nu,n'\nu'} \tilde{R}_{n\ell'}(p'), \tag{A2}$$

where the $\tilde{R}_{n\ell}(p)$ is the momentum space representation of the radial harmonic oscillator wave function. Additionally, we introduce the square root of the norm kernel $\mathcal{N}^{1/2}$ and its inverse $\mathcal{N}^{-1/2}$, which are defined such that $[\mathcal{N}^{1/2} \cdot \mathcal{N}^{1/2}]_{\nu\nu'}(p, p') \equiv \mathcal{N}_{\nu\nu'}(p, p')$ and $[\mathcal{N}^{1/2} \cdot \mathcal{N}^{-1/2}]_{\nu\nu'}(p, p') \equiv \frac{\delta(p,p')}{pp'}\delta_{\nu\nu'}$. The multiplication by the norm implies a sum over channel indices and an integral over the momentum coordinate such that, e.g.,

$$[\mathcal{N}^{1/2} \cdot \mathcal{N}^{1/2}]_{\nu\nu'}(p, p') = \sum_{\nu''} \int dp'' p''^2 \mathcal{N}_{\nu\nu''}^{1/2}(p, p'')$$

$$\times \mathcal{N}_{\nu''\nu'}^{1/2}(p'', p'). \tag{A3}$$

Further, the (inverse) square root fulfills Eq. (A2), with matrix elements $\Lambda_{n\nu,n'\nu'}^{\pm 1/2}$ replacing $\Lambda_{n\nu,n'\nu'}$ and represents the component of the norm square (inverse square) root inside the P space. To proceed, we note that the momentum space representation of the average Coulomb potential $\bar{V}^{\mathrm{c}}(r)$ is nonlocal and has an angular dependence so that $\bar{V}^{\mathrm{c}} \equiv \bar{V}_\ell^{\mathrm{c}}(p, p')$. By introducing the average Coulomb potential kernel $\mathcal{V}_{\nu\nu'}^{\mathrm{c}}(p, p') = \bar{V}_\ell^{\mathrm{c}}(p, p')\,\delta_{\nu\nu'}$ and the relative potential kernel

$$\mathcal{V}_{\nu\nu'}^{\mathrm{rel}}(p, p') \equiv \langle\Phi_{\nu p}|\mathcal{A} V^{\mathrm{rel}}\mathcal{A}|\Phi_{\nu'p'}\rangle, \tag{A4}$$

the Hamiltonian kernel can be expressed as

$$\mathcal{H}_{\nu\nu'}(p, p') = E_\nu^{(A)} \mathcal{N}_{\nu\nu'}(p, p') + \frac{p^2}{2\mu} \mathcal{N}_{\nu\nu'}(p, p')$$

$$+ [\mathcal{V}^{\mathrm{c}} \mathcal{N}]_{\nu\nu'}(p, p') + \mathcal{V}_{\nu\nu'}^{\mathrm{rel}}(p, p'). \tag{A5}$$

The $(A + 1)$-body Schrödinger equation satisfied by the NCSM/RGM wave function of Eq. (24) can thus be cast as

$$\sum_{\nu'} \int dp' p'^2 \left[E_{A+1} \mathcal{N}_{\nu\nu'}(p, p') - \mathcal{H}_{\nu\nu'}(p, p')\right]$$

$$\times [\mathcal{N}^{-1/2} \chi]_{\nu'\nu_0}(p', p_0) = 0, \tag{A6}$$

or in the condensed form

$$[E_{A+1} - \bar{\mathcal{H}}] \chi = 0, \tag{A7}$$

after multiplying by $\mathcal{N}^{-1/2}$ from the left, where the effective potential is given by $\bar{\mathcal{H}} \equiv \mathcal{N}^{-1/2} \mathcal{H} \mathcal{N}^{-1/2}$ and E_{A+1} is the total energy of the nucleon-target system. The model space Hamiltonian kernel $\bar{\mathcal{H}}^{\mathrm{mod}}$ (i.e., the component of the Hamiltonian kernel $\bar{\mathcal{H}}_{\nu\nu'}$ within the HO model space is computed similarly to the NCSM/RGM presented in Ref. [28] except that the momentum space HO wave functions are used in the place of their coordinate space counterparts. Further, there are corrections to $\bar{\mathcal{H}}_{\nu\nu'}(p, p')$ emerging from outside the model space P due to the presence of long-ranged terms in Eq. (A5), namely, the target nucleus energy eigenvalue $\mathcal{H}_{\nu\nu'}^{\mathrm{eev}}(p, p') \equiv E_\nu^{(A)} \mathcal{N}_{\nu\nu'}(p, p')$, the relative nucleon-nucleus kinetic energy $\mathcal{H}_{\nu\nu'}^{\mathrm{kin}}(p, p') \equiv E_\nu^{(A)} \mathcal{N}_{\nu\nu'}(p, p')$, and the average Coulomb potential, $\mathcal{V}_{\nu\nu'}^{\mathrm{coul}}(p, p') \equiv \delta_{\nu\nu'} [\bar{V}_\ell^{\mathrm{c}} Q_\ell]_{\nu\nu'}(p, p')$. To compute the out-of-model-space contributions to $\bar{\mathcal{H}}_{\nu\nu'}(p, p')$ arising from these terms, we multiply by $\mathcal{N}^{-1/2}$ from both sides and Hermitize (i.e., add Hermitian conjugate and multiply by $1/2$) leading to

$$\bar{\mathcal{H}}_{\nu\nu'}^{\mathrm{eev}}(p, p') = E_\nu^{(A)} \delta_{\nu\nu'} \frac{\delta(p-p')}{pp'}$$

$$\times -E_\nu^{(A)} \delta_{\nu\nu'} \sum_{n=0}^{n_{\max}} \tilde{R}_{n\ell}(p) \tilde{R}_{n\ell}(p'), \tag{A8}$$

for the energy eigenvalue term. Although the Hamiltonian kernel $\bar{\mathcal{H}}_{\nu\nu'}(p, p')$ in the full space (i.e., $n_{\max} \to \infty$) is Hermitian, the representation at finite $n_{\max}$ does not fulfill this symmetry and therefore necessitates the explicit Hermitization. Additionally, the kinetic energy

term gives

$$\bar{\mathcal{H}}^{\mathrm{kin}}_{\nu\nu'}(p, p') = \frac{p^2}{2\mu}\,\delta_{\nu\nu'}\,\frac{\delta(p - p')}{pp'} - \frac{p^2}{2\mu}\,\delta_{\nu\nu'}\sum_{n=0}^{n_{\max}}\sum_{n'=0}^{n_{\max}}\tilde{R}_{n\ell}(p)\,T_{\ell,nn'}\,\tilde{R}_{n\ell}(p')$$

$$- \sum_{n=0}^{n_{\max}}\tilde{R}_{n_{\max}+1,l}(p)\,T_{\ell,n_{\max}+1,n_{\max}}\left[\delta_{\nu\nu'}\,\delta_{nn_{\max}} - \frac{1}{2}\Lambda^{-1/2}_{n\nu,n_{\max}\nu'} - \frac{1}{2}\Lambda^{1/2}_{n\nu,n_{\max}\nu'}\right]\tilde{R}_{n\ell}(p)$$

$$- \sum_{n=0}^{n_{\max}}\tilde{R}_{n\ell'}(p')\left[\delta_{\nu\nu'}\,\delta_{nn_{\max}} - \frac{1}{2}\Lambda^{-1/2}_{n_{\max}\nu,n\nu'} - \frac{1}{2}\Lambda^{1/2}_{n_{\max}\nu,n\nu'}\right]T_{\ell,n_{\max},n_{\max}+1}\tilde{R}_{n_{\max}+1,l}(p), \tag{A9}$$

where $T_{\ell,nn'} \equiv \langle R_{n\ell}|\,p^2/2\mu\,|R_{n'\ell}\rangle$ are the kinetic energy matrix elements in the HO basis. The first term in Eq. (A8) and Eq. (A9) is, respectively, the energy eigenvalue of the target nucleus and the relative nucleon-target kinetic energy. The remaining terms constitute the respective contributions to the effective nucleon-target potential $\mathcal{W}^{\mathrm{eev}}_{\nu\nu'}(p, p')$ and $\mathcal{W}^{\mathrm{kin}}_{\nu\nu'}(p, p')$, such that

$$\bar{\mathcal{H}}^{\mathrm{eev}}_{\nu\nu'}(p, p') = E_\nu^{(A)}\,\delta_{\nu\nu'}\,\frac{\delta(p - p')}{pp'} + \mathcal{W}^{\mathrm{eev}}_{\nu\nu'}(p, p'), \tag{A10}$$

and

$$\bar{\mathcal{H}}^{\mathrm{kin}}_{\nu\nu'}(p, p') = \frac{p^2}{2\mu}\,\delta_{\nu\nu'}\,\frac{\delta(p - p')}{pp'} + \mathcal{W}^{\mathrm{kin}}_{\nu\nu'}(p, p'). \tag{A11}$$

Additionally, the correction due to the average Coulomb potential is given by

$$\bar{\mathcal{H}}^{\mathrm{coul}}_{\nu\nu'}(p, p') = \bar{V}^{\mathrm{c}}_\ell(p, p')\,\delta_{\nu\nu'} + \sum_{n=0}^{n_{\max}}\sum_{n'=0}^{n_{\max}}\left(\tilde{R}_{n\ell}(p)\,\langle R_{n'\ell'}|\,\bar{V}^{\mathrm{c}}_\ell\,|p'\rangle + \langle p|\,\bar{V}^{\mathrm{c}}_\ell\,|R_{n\ell}\rangle\tilde{R}_{n'\ell'}(p')\right)\left(\frac{1}{2}\,\Lambda^{-1/2}_{n\nu,n'\nu'} - \delta_{\nu\nu'}\,\delta_{nn'}\right)$$

$$+ \sum_{n=0}^{n_{\max}}\sum_{n'=0}^{n_{\max}}R_{n\ell}(p)\,R_{n'\ell'}(p')\left(\delta_{\nu\nu'}\,\tilde{V}^{\mathrm{c}}_{\ell,nn'} - \frac{1}{2}\sum_{n''=0}^{n_{\max}}\left(\tilde{V}^{\mathrm{c}}_{\ell,nn''}\Lambda^{-1/2}_{n''\nu,n'\nu'} + \Lambda^{-1/2}_{n\nu,n''\nu'}\tilde{V}^{\mathrm{c}}_{\ell,n''n'}\right)\right), \tag{A12}$$

where $\tilde{V}^{\mathrm{c}}_{\ell,nn''} \equiv \langle R_{n\ell}|\bar{V}^{\mathrm{c}}_\ell|R_{n''\ell}\rangle$ are the matrix elements of average Coulomb potential in the HO basis. The full nucleon-target potential is therefore given by the sum

$$\mathcal{W}_{\nu\nu'}(p, p') = \bar{\mathcal{H}}^{\mathrm{mod}}_{\nu\nu'}(p, p') + \mathcal{W}^{\mathrm{eev}}_{\nu\nu'}(p, p') + \mathcal{W}^{\mathrm{kin}}_{\nu\nu'}(p, p') + \bar{\mathcal{H}}^{\mathrm{coul}}_{\nu\nu'}(p, p'), \tag{A13}$$

and the full Hamiltonian kernel takes the form

$$\bar{\mathcal{H}}_{\nu\nu'}(p, p') = \left[E_\nu^{(A)} + \frac{p^2}{2\mu}\right]\delta_{\nu\nu'}\,\frac{\delta(p - p')}{pp'} + \mathcal{W}_{\nu\nu'}(p, p'), \tag{A14}$$

which is substituted into Eq. (A7) to arrive at the effective two-body Schrödinger in momentum space. Finally, we can write Eq. (A7) explicitly leading to

$$\left[E_{A+1} - E_\nu^{(A)} - \epsilon_\nu - \frac{p^2}{2\mu}\right]\chi_{\nu\nu_0}(p, p_0) = \sum_{\nu'}\int dp'\,p'^2\,\mathcal{W}_{\nu\nu'}(p, p')\,\chi_{\nu'\nu_0}(p', p_0). \tag{A15}$$

We note that the quantity $E_{A+1} - \bar{\mathcal{H}}$ contains the difference $E_{A+1} - E_\nu^{(A)}$, which is the total energy of the $(A + 1)$ system relative to the energy of the target nucleus. It is customary to define an incident relative kinetic energy $E_{\mathrm{kin}} \equiv E_{A+1} - E_{\nu_0}^{(A)}$ so that the relative kinetic energy has the form energy $E_{A+1} - E_\nu^{(A)} = E_{\mathrm{kin}} - \epsilon_\nu$. The corresponding t matrix fulfills the Lippmann-Schwinger (LS) equation

$$t_{\nu\nu_0}(p, p_0; E_{\mathrm{kin}}) = \mathcal{W}_{\nu\nu_0}(p, p_0) + \sum_{\nu'}\int dp'\,p'^2\,\mathcal{W}_{\nu\nu'}(p, p')\,G_{0\nu'}(E_{\mathrm{kin}}, p')\,t_{\nu\nu_0}(p', p_0; E_{\mathrm{kin}}). \tag{A16}$$

which is equivalent to Eq. (A15) complemented by the scattering boundary conditions, and the propagator is given by $G_{0\nu'}(E_{\mathrm{kin}}, p') = [E_{\mathrm{kin}} - \epsilon_{\nu'} - p'^2/2\mu + i0]^{-1}$.

---

[1] G. Hupin, S. Quaglioni, and P. Navrátil, Nat. Commun. **10**, 351 (2019).

[2] F. Raimondi, G. Hupin, P. Navrátil, and S. Quaglioni, Phys. Rev. C **93**, 054606 (2016).

[3] L. D. Faddeev, Sov. Phys. JETP **12**, 1014 (1961).

[4] R. C. Johnson and P. J. R. Soper, Phys. Rev. C **1**, 976 (1970).

[5] R. C. Johnson and P. C. Tandy, Nucl. Phys. A **235**, 56 (1974).

[6] M. Yahiro, Y. Iseri, H. Kameyama, M. Kamimura, and M. Kawai, Prog. Theor. Phys. Suppl. **89**, 32 (1986).

[7] R. Machleidt, K. Holinde, and C. Elster, Phys. Rep. **149**, 1 (1987).

[8] R. Machleidt, Phys. Rev. C **63**, 024001 (2001).

[9] D. R. Entem and R. Machleidt, Phys. Rev. C **68**, 041001(R) (2003).

[10] D. R. Entem, N. Kaiser, R. Machleidt, and Y. Nosyk, Phys. Rev. C **91**, 014002 (2015).

[11] E. Epelbaum, H. Krebs, and U. G. Meißner, Phys. Rev. Lett. **115**, 122301 (2015).

[12] A. Deltuva, A. C. Fonseca, and P. U. Sauer, Phys. Rev. C **73**, 057001 (2006).

[13] A. Deltuva, Nucl. Phys. A **821**, 72 (2009).

[14] J. Lei, L. Hlophe, C. Elster, A. Nogga, F. M. Nunes, and D. R. Phillips, Phys. Rev. C **98**, 051001(R) (2018).

[15] L. J. Titus and F. M. Nunes, Phys. Rev. C **89**, 034609 (2014).

[16] P. Doleschall, Phys. Rev. C **77**, 034002 (2008).

[17] H. Feshbach, Annu. Rev. Nucl. Sci. **8**, 49 (1958).

[18] A. Deltuva, Phys. Rev. C **79**, 021602(R) (2009).

[19] R. J. Charity, J. M. Mueller, L. G. Sobotka, and W. H. Dickhoff, Phys. Rev. C **76**, 044314 (2007).

[20] A. A. Ioannides and R. C. Johnson, Phys. Rev. C **17**, 1331 (1978).

[21] R. Johnson, J. Tostevin, and M. Lopes, Nucl. Phys. 1980, 750 (1981).

[22] R. C. Johnson, N. Austern, and M. H. Lopes, Phys. Rev. C **26**, 348 (1982).

[23] J. Tostevin, M. Lopes, and R. Johnson, Nucl. Phys. A **465**, 83 (1987).

[24] M. J. Dinmore, N. K. Timofeyuk, J. S. Al-Khalili, and R. C. Johnson, Phys. Rev. C **99**, 064612 (2019).

[25] M. Theeten, H. Matsumura, M. Orabi, D. Baye, P. Descouvemont, Y. Fujiwara, and Y. Suzuki, Phys. Rev. C **76**, 054003 (2007).

[26] S. K. Bogner, R. J. Furnstahl, and R. J. Perry, Phys. Rev. C **75**, 061001(R) (2007).

[27] S. Quaglioni and P. Navratil, Phys. Rev. Lett. **101**, 092501 (2008).

[28] S. Quaglioni and P. Navratil, Phys. Rev. C **79**, 044606 (2009).

[29] A. Deltuva, Phys. Rev. C **74**, 064001 (2006).

[30] N. J. Upadhyay, A. Deltuva, and F. M. Nunes, Phys. Rev. C **85**, 054621 (2012).

[31] L. Hlophe, A. Deltuva, C. Elster, F. M. Nunes, and S. Quaglioni (unpublished).

[32] E. O. Alt, P. Grassberger, and W. Sandhas, Nucl. Phys. B **2**, 167 (1967).

[33] A. M. Mukhamedzhanov, V. Eremenko, and A. I. Sattarov, Phys. Rev. C **86**, 034001 (2012).

[34] L. Hlophe, J. Lei, C. Elster, A. Nogga, and F. M. Nunes, Phys. Rev. C **96**, 064003 (2017).

[35] A. M. Mukhamedzhanov, E. O. Alt, and G. V. Avakov, Phys. Rev. C **61**, 064006 (2000).

[36] D. J. Ernst, C. M. Shakin, and R. M. Thaler, Phys. Rev. C **8**, 46 (1973).

[37] A. M. Mukhamedzhanov, E. O. Alt, and G. V. Avakov, Phys. Rev. C **63**, 044005 (2001).

[38] M. Gell-Mann and M. L. Goldberger, Phys. Rev. **91**, 398 (1953).

[39] D. J. Ernst, C. M. Shakin, R. M. Thaler, and D. Weiss, Phys. Rev. C **8**, 2056 (1973).

[40] L. Hlophe, Ch. Elster, R. C. Johnson, N. J. Upadhyay, F. M. Nunes, G. Arbanas, V. Eremenko, J. E. Escher, and I. J. Thompson (The TORUS Collaboration), Phys. Rev. C **88**, 064608 (2013).

[41] The TORUS Collaboration, L. Hlophe, V. Eremenko, C. Elster, F. M. Nunes, G. Arbanas, J. E. Escher, and I. J. Thompson, Phys. Rev. C **90**, 061602(R) (2014).

[42] L. Hlophe and C. Elster, Phys. Rev. C **93**, 034601 (2016).

[43] L. Hlophe, J. Lei, C. Elster, A. Nogga, F. M. Nunes, D. Jurčiukonis, and A. Deltuva, Phys. Rev. C **100**, 034609 (2019).

[44] J. Bang, J. J. Benayoun, C. Gignoux, and I. J. Thompson, Nucl. Phys. A **405**, 126 (1983).

[45] M. Hesse, J. M. Sparenberg, F. Van Raemdonck, and D. Baye, Nucl. Phys. A **640**, 37 (1998).

[46] M. Hesse, J. Roland, and D. Baye, Nucl. Phys. A **709**, 184 (2002).

[47] P. Navratil and S. Quaglioni, Phys. Rev. C **83**, 044609 (2011).

[48] P. Navrátil, S. Quaglioni, G. Hupin, C. Romero-Redondo, and A. Calci, Phys. Scr. **91**, 053002 (2016).

[49] G. Hupin, S. Quaglioni, and P. Navrátil, Phys. Rev. C **90**, 061601(R) (2014).

[50] I. J. Barit, Balashko, L. Ju. G., Dulkova, and V. P. Zavarzina, Sov. J. Nucl. Phys. **29**, 585 (1979).

[51] G. Hupin, S. Quaglioni, and P. Navrátil, Phys. Rev. Lett. **114**, 212502 (2015).